Flow of simple liquids down narrow V grooves

J. A. Mann, Jr.,[1] L. Romero,[2] R. R. Rye,[2] and F. G. Yost[2]
[1]*Case Western Reserve University, Cleveland, Ohio 44106*
[2]*Sandia National Laboratories, Albuquerque, New Mexico 87185*
(Received 27 January 1995)

The dynamics of spreading of simple liquids down straight, narrow V grooves open at the top were captured by real-time video imaging. Groove depths in polished copper ranged between 40 and 100 μm and extended approximately 2 cm with V angles of 30°, 60°, and 90°. The surface tension to viscosity ratios ranged from 46 to 970 cm/sec and the capillary number was small, Ca $\ll 1$ in all cases. The length of the spreading liquid scaled with $\sqrt{t}$ accurately for every case examined; the dynamics were well represented by two numbers, the location of the front in reduced coordinates and a diffusion coefficient. A simple theory is presented for the dynamics of the advancing front that requires no adjustable parameters and fits well the experimental data collected with six alcohols. Unlike drop spreading, the *ad hoc* slip boundary condition of that theory is not invoked for the open groove problem; only the static advancing contact angle is used.

PACS number(s): 68.45.Gd, 68.45.Kg, 83.50.Lh

INTRODUCTION

The kinetics of liquid flow through capillary tubes has been studied for over a century [1,2], and much of the renewed interest is motivated by the similarity to flow in random porous media, wherein an ensemble of contorted capillarities is used as a model system [3–5]. Similarly, the spreading of a thin liquid film over a rough surface can be thought of as channel flow through a random network of contiguous V grooves. For example, a tin-lead alloy on rough copper surfaces [6] can flow extensively and with uncommon rapidity. This paper represents a systematic examination of simple liquids (nonreacting) spreading along well characterized, open grooves; experimental and theoretical results are reported and show excellent agreement

We show that a simple continuum model of flow is satisfactory for understanding the open-channel capillary behavior of liquids that exhibit a range of surface tension to viscosity ratios (γ/μ) and contact angles (θ); see Fig. 1(a). The range of these parameters, listed in Table I, is enough to show that a simple fluid dynamic model is sufficient to represent the experimental data. No adjustable parameters are required, nor is any slip boundary condition necessary. It is demonstrated that the kinetic data scale as $\sqrt{\gamma/\mu}$ and as h_0 (groove depth). It is also demonstrated that the liquid profile scales as $\eta = z/\sqrt{Dt}$, where z is the distance down the groove, D is a type of diffusion coefficient, and t is flow time; see Fig. 1(b).

EXPERIMENT

An experimental problem is to machine grooves that conform closely to the mathematical model, shown in Fig. 1(a). The V grooves were scribed on polished copper using carefully ground and polished pieces of machine tool steel with three angles (β) of 30°, 60°, and 90°. Each of six polished copper blanks of approximately $2.5 \times 2.5 \times 0.3$ cm were scribed with a set of three intersecting grooves, each with a different groove angle β. Different depths (from 40 to 100 μm) were obtained depending on the angle. The scribing left ridges on the grooves that were subsequently polished flat. We determined the shape of the grooves, as well as the depths, by

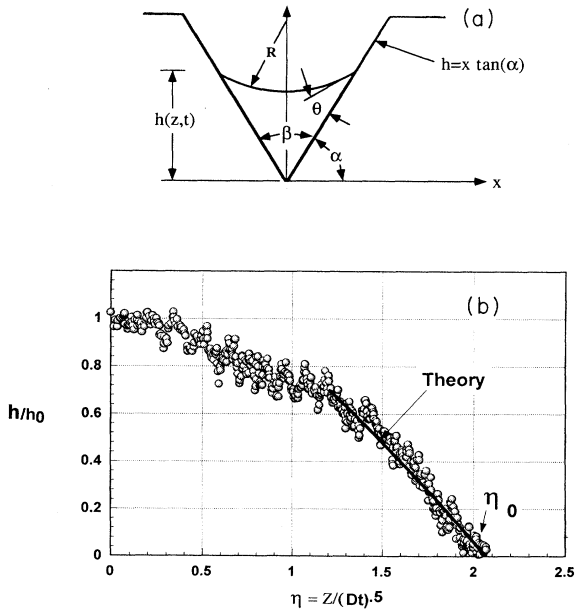

FIG. 1. (a) shows the groove cross section with the geometrical parameters identified. The axis of the channel, z, is perpendicular to the plane of the figure. (b) shows the experimental height variation along a $\beta = 60°$ groove as determined by intensity measurements for spreading cyclohexanol. Data from six profiles at 2.5, 5, 8.8, 12.6, 16.9, and 26.7 sec after t_0 were scaled in terms of reduced coordinates and plotted together. A three-point running average was used to attenuate variations from pixel to pixel due to noise.

TABLE I. Experimental parameters, and experimental and calculated kinetic rate data.

Liquid	γ/μ (cm/sec)	Contact angle (deg)	Groove height (μm)	Expt. η_0	Theor. η_0	Theor. $K(\alpha,\theta)$	Theor. rate[a] (cm/sec$^{1/2}$)	Calc. rate[b] (cm/sec$^{1/2}$)	Expt. rate (cm/sec$^{1/2}$)	Percent diff.[b]
1-4-butadiol	63.1	29	91	1.4	2.4	0.0216	0.267	0.156	0.180	+13
cyclohexanol	45.8	6	91	2.0	2.65	0.0233	0.262	0.197	0.200	+1.5
1-butanol	969	6	91	2.0	2.65	0.0233	1.20	0.905	0.861	−5.1
2-octanol	408	<2	91	2.0	2.65	0.0222	0.763	0.574	0.574	+0.0
diethylene-glycol	115	33	91	1.4	2.4	0.0202	0.347	0.203	0.227	+10.6
1-heptanol	390	<2	91	2.0	2.65	0.0222	0.746	0.561	0.591	+5.1
cyclohexanol	45.8	6	55	2.0	2.65	0.0233	0.204	0.153	0.139	−10.1
cyclohexanol	45.8	6	57	2.0	2.65	0.0233	0.208	0.156	0.163	+4.3
cyclohexanol	45.8	6	91	2.0	2.65	0.0233	0.262	0.197	0.200	+1.5
cyclohexanol	45.8	6	86	2.0	2.65	0.0233	0.254	0.191	0.195	+2.1
cyclohexanol	45.8	6	83	2.0	2.65	0.0233	0.250	0.188	0.187	−0.5

[a]Calculated using theoretical values for both D and η_0.
[b]Calculated using the theoretical value for D and the experimental value for η_0.

two techniques: a Dektak-8000 profilometer and a Wyko (MHT-II) vertical scanning interferometer. The tip of the profilometer had a cone angle of 60°, which allowed reasonable accuracy in characterizing the 90° grooves but could only give the width of the opening of the 60° and 30° grooves. Dental impression material was used to form an image of the grooves that could then be profiled to find the depth of the grooves; see Table I. The Wyko instrument confirmed the depth data and provided accurate profile information for all grooves.

The liquids listed in Table I were used as received and literature values [7] for the surface tensions, and viscosities were used in the interpretation of the spreading data. Advancing static contact angles were measured by observing the profiles of sessile drops of the various liquids in Table I, an uncertainty of about 2° was maintained. We were able to greatly increase the contrast in the video images by spiking each liquid with a very small mole fraction of the fluorescing dye coumarin. A "black-light" gave images of good contrast between the spreading liquid that fluoresced and the copper substrate that was only weakly illuminated by the "black-light."

Spreading experiments, starting from a small drop of liquid placed on the crossing of the grooves, were recorded in real time by a 512×512 pixel charge-coupled-device camera attached to a zoom lens. A Sony video recorder was fitted with time base electronics so that a time stamp was recorded on each image. The system operated at 30 frames per sec timed to better than 0.01 sec. An Image Pro system with a frame grabber was used to produce image files for further processing. Spreading lengths (the edge of the drop to the wet-to-dry edge of the advancing front) were measured in each frame using image analysis software. Typical results are shown in Fig. 2 for the six liquids used in this study. When spreading occurred we found that the distance of the front down any groove, for any liquid, was accurately linear with $\sqrt{t}$ starting a few frames after the liquid entered a groove. This is a major experimental result and is consistent with capillary flow kinetics in closed capillaries [2].

It was also possible to determine the profile of the spreading liquid in detail using TIFF files captured from the videotape record of the spreading dynamics by measuring the intensity of the fluorescence along the line of pixels down the center of the filling grove. The ratio

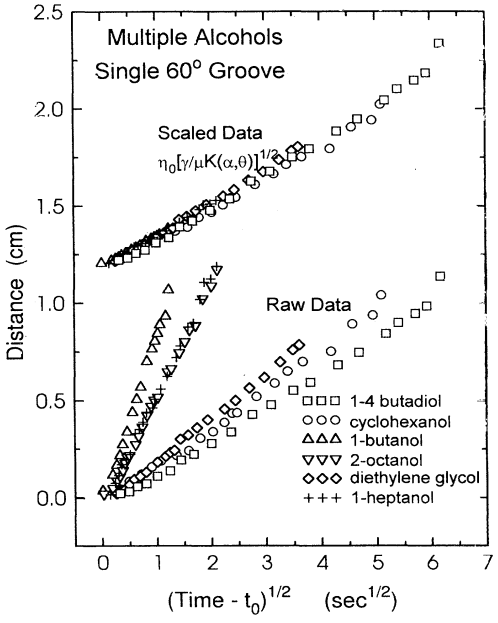

FIG. 2. Linear plots of the data sets as spreading distance vs the square root of spreading time. Lower set of curves: raw experimental data. Upper set of curves: result of scaling of the experimental data to that of 1-4-butadiol using the data in Table I and $\eta_b[\gamma/\mu K(\alpha,\theta)]^{1/2}$ as a scaling factor. The experimental rates in Table I are obtained from least squares fits to the experimental data.

h/h_0 was estimated by the intensity ratio I/I_0, where $I(z,t)$ was the gray-scale level at (z,t) and I_0 was the gray-scale level at the edge of the drop at the front of the groove; see Fig. 1(b). The frame grabbing process added some noise to the images, which was minimized by doing a three-point running average on the raw data. We now describe the elements of a theory that represents the spreading kinetics without adjustable parameters and then discuss the comparison with the experimental results shown in the figures and table.

MODEL

Consider a V-shaped groove, as shown in Fig. 1(a). The wetting liquid defines a contact angle $\theta(z,t)$ with the straight walls of the groove that are oriented at an angle α relative to the surface of the plate. Liquid fills the groove to a depth $h(z,t)$. The free-liquid surface is assumed to have a circular shape with radius R, and z is the axial position along the groove with the origin at the edge of the liquid drop. The depth of the liquid at $z=0$ is h_0. The source of the wetting liquid is a sessile drop having radius $R_0 \gg R$, large enough so that its Laplace pressure can be ignored and the location of its three-phase contact line is nearly constant with time. Flow commences at time $t=0$, and the liquid is drawn into the groove by capillary forces to a distance $z_0(t)$ from the three-phase contact line of the sessile drop. The mathematical problem is to calculate the flow distance and the shape of the liquid in this perfect V groove as a function of time.

The pressure drop across the surface at a distance z down the groove is given by the Laplace equation

$$0=\gamma\left[\frac{1}{R}+\frac{1}{R_2}\right]-\mathbf{n}\cdot[\mathbf{P}]\cdot\mathbf{n}\ , \tag{1}$$

where γ is liquid surface tension, R_2 is the radius of curvature along z, $[\mathbf{P}]$ is the pressure tensor jump, and $\mathbf{n}$ is the normal vector to the liquid surface. In $\mathbf{P}$, the contribution due to the velocity gradient at the free surface is ignored because it is small, which is justified by the fact that the capillary number is small, $\mathrm{Ca}=U(\mu/\gamma)\ll 1$, where U is a characteristic velocity. Experimentally, $\mathrm{Ca}<0.0006$. Later in this paper we provide experimental evidence that $R2\gg R$, allowing $1/R_2$ to be safely neglected for our modeling purposes. If $1/R_2$ is neglected in Eq. (1) relative to $1/R$, the pressure in the fluid is given as

$$p(\alpha,z,t)=-\gamma\frac{\sin[\alpha-\theta(z,t)]\tan(\alpha)}{h(z,t)}+p_0\ , \tag{2}$$

where p_0 is the constant pressure in the vapor phase. The gradient of this pressure is the driving force for the flow.

The pressure may vary down the groove through both h and θ. The simplification we use is to consider the flow as occurring in two segments. In the first segment, the liquid fills the groove $h(z,t)=h_0$, extending up to some location behind the advancing front. Over the distance of the filled groove where the liquid is pinned at the edges of the groove, h is constant and the pressure variation is through $\theta(z,t)$. The pressure variation in the second segment, which is the unfilled region that includes the front, is through $h(z,t)$ with fixed θ. In the second segment θ is taken as the advancing, static contact angle. We next construct the governing equation for the variation of $h(z,t)$ down the unfilled segment of the groove. The problem of flow in both segments, including matching conditions, is the focus of a second paper [8].

The volumetric flow rate q is related to the cross sectional area $A(z,t)$ of the liquid by the formula

$$\frac{\partial q(z,t)}{\partial z}=-\frac{\partial A(z,t)}{\partial t}\ , \tag{3}$$

which was derived from mass conservation in the thin shell $(z,z+\delta)$ of volume $A^*\delta$ assuming that the liquid is incompressible. The cross sectional area of the liquid in the groove, Fig. 1(a), is

$$A(\alpha,z,t)=h(z,t)^2A^*[\alpha,\theta(z,t)]\ , \tag{4}$$

where

$$A^*(\alpha,\theta)=\frac{\sin^2(\alpha-\theta)\tan(\alpha)-(\alpha-\theta)+\sin(\alpha-\theta)\cos(\alpha-\theta)}{\tan^2(\alpha)\sin^2(\alpha-\theta)}\ .$$

The volumetric flow rate can be written in the convenient form [8]

$$q=-\frac{h^4(z,t)}{\mu}\Gamma(\theta,\alpha)\frac{\partial p}{\partial z}\ , \tag{5}$$

where $\Gamma(\theta,\alpha)$ is a positive function that plays the role of an area-averaged velocity field along the groove and μ is the liquid viscosity. The pressure gradient along the axis of the groove is assumed to change on a length scale that is large compared to $h(z,t)$. Combining Eqs. (2)–(5) with θ constant (unfilled groove) we find that the governing partial differential equation is of the diffusion type

$$\frac{\partial}{\partial t}h^2(z,t)=\frac{D}{h_0}\frac{\partial}{\partial z}\left[h^2(z,t)\frac{\partial h(z,t)}{\partial z}\right]\ , \tag{6a}$$

where by definition

$$D=\frac{\gamma}{\mu}h_0K(\alpha,\theta)=\frac{\gamma}{\mu}h_0\frac{\Gamma(\alpha,\theta)\sin(\alpha-\theta)\tan(\alpha)}{A^*(\alpha,\theta)}\ . \tag{6b}$$

Relevant $K(\alpha,\theta)$ numbers are listed in Table I. This is an ill-posed problem if the diffusion coefficient is negative

but well posed if $D>0$, necessarily $\alpha-\theta>0$. If $\theta<\pi/2$, flow will commence if α is large enough. We solve Eq. (6a) in the front segment and a similar equation in the back segment. The solutions are matched by requiring that the pressure and pressure gradients are continuous at the dividing surface between the two segments of the groove. We also assume initial and boundary conditions $h(z,0)=0$ and that $\theta\to\alpha$ as $z\to 0$. We use the fact that at any finite time, the total volume of liquid in the groove is finite, so that for $t<\infty$, $\int_0^\infty h^2(z,t)dz<\infty$.

Observe that the governing equation and initial and boundary conditions are invariant to the transformation $z=\lambda z$, $t=\lambda^2 t$. This invariance ensures that from Eq. (6a) the similarity variable is

$$h(z,t)=h_0\phi(\eta)\ , \tag{7}$$

where

$$\eta=\frac{z}{\sqrt{Dt}}\ . \tag{8}$$

See Ref. [9] for many details and examples.

A special case of Eq. (8) is used in computing the rate constants shown in Table I: the distance to the front is z_0 and the corresponding scaled distance is η_0. The experimental rate constant, the slope of z_0 vs $\sqrt{t}$, is compared to $\eta_0\sqrt{D}$, the calculated rate constant in Table I. The coefficient D is insensitive to the details of the model for the first segment of the flow and so is used in the experimental estimate of η_0, which is somewhat sensitive to how the contact angle variation is modeled. Theoretical values of η_0 for wetting liquids ($\theta\sim 0$) range from 1.7 when the groove is never filled to 2.6 for the two segment model. D is calculated from Eq. (6) using the static, advancing contact angle.

Several details are omitted which we plan to publish elsewhere [8]. For example, the function $\Gamma(\alpha,\theta)$ is defined as part of the process of constructing q, Eq. (5), and developing numerical solutions of the boundary value problem. Such numerical solutions are necessary to determine values for $K(\alpha,\theta)$ in Eq. (6b) and η_0. There is no exact analytical representation in terms of simple functions. Approximation formulas [8], which reproduce the numbers for $K(\alpha,\theta)$ used in Table I, are

$$\Gamma(\alpha,\theta)=\Gamma(\alpha,\alpha)\left[\frac{h_{cl}}{h_0}\right]^3\left[\frac{A^*(\theta,\alpha)}{\cot\alpha}\right]^{1/2}\ ,$$

$$\frac{h_{cl}}{h_0}=1+\frac{\cot\alpha[\cos(\alpha-\theta)-1]}{\sin(\alpha-\theta)}\ , \tag{9a}$$

$$\Gamma(\alpha,\alpha)=\frac{\frac{1}{6}\cot^3\alpha+\frac{3.4}{6}\cot^4\alpha+\frac{1}{6}\cot^5\alpha}{1+3.4\cot\alpha+4\cot^2\alpha+3.4\cot^3\alpha+\cot^4\alpha}\ . \tag{9b}$$

Formula (9) is accurate to 2.5% when compared to the numerical solution of the boundary value problem and is valid for both segments.

RESULTS AND DISCUSSION

We assert that the spreading distance is linear with $\sqrt{t}$. This contention is supported by the experimental data shown in Fig. 2, which demonstrate the linear relationship between z_0 and $\sqrt{t-t_0}$, where t_0 is the time associated with the frame in which the liquid is first seen in the groove. (It was difficult to determine t_0 exactly from the video record.) Also note that there are deviations when t goes to t_0, which is expected since the flow fields are not well developed at times close to t_0. (A log-log plot of the data is linear, except at short times.) We also tested the hypothesis of $\sqrt{t}$ behavior by fitting on the test function $z_0=a(t-t_0)^n$, allowing n to adjust to a nonlinear least squares fit to determine a, t_0, and n. The results are that for six liquids $n=0.521\pm 0.04$. However, the linear estimate of the correlation coefficient between a and n was greater than -0.9 and as large as -0.99, which signals a strong correlation of these parameters when fit to the data. A second set of fits adjusted a, t_0 but kept $n=\frac{1}{2}$. The weighted sum of the squares of the residuals are very close to being the same regardless of whether n is adjusted or fixed at $n=\frac{1}{2}$. The result of this nonlinear least squares fitting is shown graphically in Fig. 3 for one example, the spreading of 1-butanol in a 60° groove. Note the indistinguishable difference compared to experiment between the case where n is fixed at $\frac{1}{2}$ and the case where n is allowed to vary. From log-log plots, nonlinear least squares fits, and the $\sqrt{t}$ plots in Fig. 2 we conclude that the hypothesis that $n=\frac{1}{2}$ is supported by all of the spreading data reported herein.

The lower portion of Fig. 2 shows the data plotted as the spreading distance vs $\sqrt{t}$ [Eq. (8)] for all six liquids

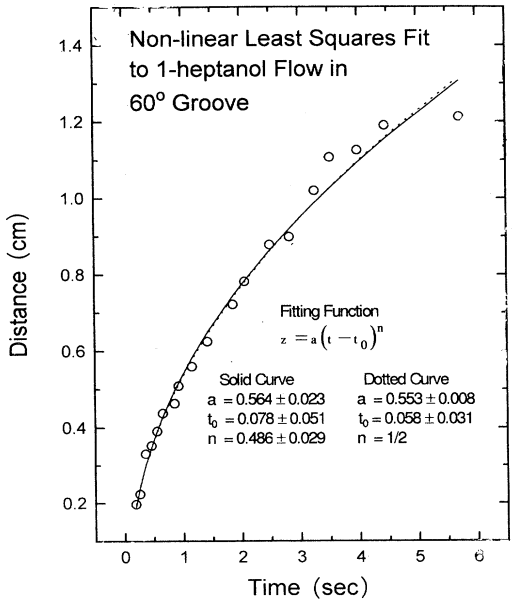

FIG. 3. Nonlinear least squares fit to 1-butanol flow in a 60° groove. The experimental data pairs (z,t) for the data in Fig. 2 were fit to the function $z=a(t-t_0)^n$. The resulting fitting parameters are given in the figure. The standard deviations were computed from each covariance matrix computed in the fit.

flowing in the same 60° groove of one of the six copper samples. The experimental rate values in Table I are the slopes (obtained from least squares fits to this data) of these experimental linear plots. This $\sqrt{t}$ dependence was always obeyed, when spreading occurred, for all combinations of sample, groove, and liquid. We observed cases where the contact angle was large enough to prevent flow, which is in qualitative agreement with the requirement that $D>0$. In fact, the fluids with contact angles clustered near 30° would not flow down the grooves in copper with $\alpha=45°$. However, the simple theory expressed here allows flow in groove angles up to 45°. Requiring $D>0$ is necessary, but a stability argument is consistent with the experimental result and may provide a sufficient condition for flow to start. Recognize that the simple theory is not valid at very short times. However, $\sqrt{t}$ behavior was established within two or three video frames ($\sim$0.1 sec) so that this limitation was not studied.

The curves in the upper portion of Fig. 2 are the result of scaling (relative to that of 1-4-butadiol) the raw data in the lower portion of the figure using $\eta_0[K(\alpha,\theta)\gamma/\mu]^{1/2}$ as the scaling factor and the values listed in Table I. Since in this case h_0 is constant, only the surface tension to the viscosity ratio and the calculated values of $K(\alpha,\theta)$ and η_0 are involved in the collapse of the experimental family of spreading rate curves to a common straight line, in this case that of 1-4-butadiol. The complementary case is where a single liquid spreads down the same type of Cu grooves. In this case $\eta_0[K(\alpha,\theta)\gamma/\mu]^{1/2}$ should be constant, leaving only h_0 as an active parameter. The lower portion of Fig. 4 contains plots of spreading distance vs $\sqrt{t}$ for cyclohexanol flowing in the 60° grooves in all six of the copper samples. Again, the corresponding experimental data values given in Table I were obtained from the slopes of this data. While the variation in groove depths is insufficiently broad to adequately test such scaling, the result of scaling of this data to $h_0^{1/2}$, as in the upper portion of Fig. 4, is clustering of the data more tightly about a single, linear relationship. This behavior is consistent with theory, as is shown quantitatively in Table I.

The profile function shown in Fig. 1(b) continues the pattern of agreement between experiment and theory and shows additional detail. The data used to generate this figure was constructed from six frames captured at different times during spreading of cyclohexanol down a 60° groove. The original data sets were first made nondimensional by the scaling of Eq. (8), then all of them were concatenated into one data set, and finally smoothed gently by a three-point running average. Figure 1(b) shows the comparison of the profile data with theory for cyclohexanol. It is clear that a single curve is traced from which an experimental η_0 was estimated for Table I.

The experimental profile is gentle, as is required for ignoring the curvature along the groove R_2. The measured angle between a tangent to the liquid surface and the groove axis was never larger than $\sim$10°. Figure 1(b) also shows the fit of the theoretical profile of the front to the experimental profile. The shape of the low contact angle front is well represented by the theory. As an additional

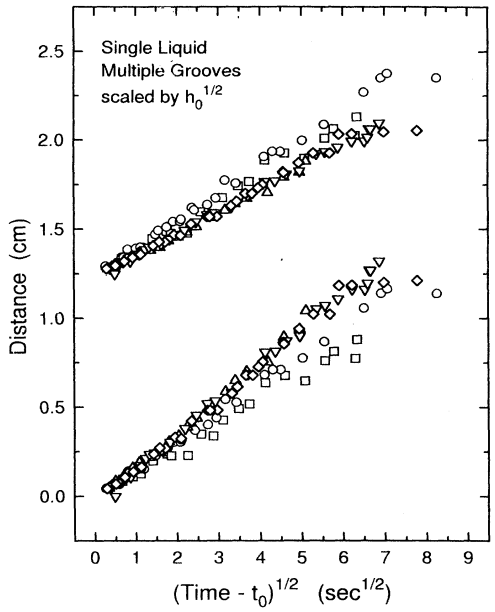

FIG. 4. Linear plots of spreading distance vs the square root of spreading time for the same alcohol (cyclohexanol) flowing in multiple examples of 60° grooves. Lower family of curves: raw experimental data. Upper family curves: result of scaling to a common groove depth using h_0 as the scaling factor. Symbols refer to the six cyclohexanol runs listed in Table I.

test, our theory predicts that in the limit as $h\to 0$, $[-(1/\eta)(\partial\phi/\partial\eta)]\to\frac{1}{2}$. The profile data was fit by a polynomial from which a rough estimate of this limit was computed. The experimental limit is 0.61 ± 0.2, which we consider to be in good agreement with theory. However, the numbers computed from theory for η_0 are too large, for example, 2.6 compared to 2.0 ± 0.2; see Table I.

The continuum theory and experiment compare well without adjustable parameters. The scaling required of this theory is established within 0.1 sec after the front emerges from the drop. At this level of theoretical development, there is no need to include a slip boundary condition at the three phase contact line as was done in the hydrodynamic theory of spreading drops [10]. When the R_2 contribution is added to Eq. (2), the modified Eq. (6a) will no longer admit a similarity solution. Inclusion of R_2 thus makes the modeling much more complex, and construction of such a model does not seem warranted by the data. Indeed, the experimental results strongly support the $\sqrt{t}$ behavior consistent with ignoring R_2. This is also consistent with the observations shown in Fig. 1(b). It appears that the R_2 term cannot be a factor in improving the estimation of η_0. We conclude that the static contact angle is sufficient for open-groove flow of many wetting liquids. The experimental data is sufficiently rich to uncover the difference between the experimental and theoretical values of η_0. Otherwise, there is essential agreement between theory and experiment. The remaining discrepancy probably involves details concerning the matching conditions between the two segments, the effect of real groove geometry, and the details

of the dynamics of the three-phase contact line at the front. These factors are being studied so as to improve the estimation of η_0. The character of the transition between the dynamics of spreading down grooves and drop spreading ($\beta = 180°$) leads to comparisons with the classical wetting literature. We plan to discuss these topics in a longer paper.

ACKNOWLEDGMENTS

R.R.R. wishes to thank G. M. Yarbrough, DDS for the use of his dental impression equipment. This work was performed at Sandia National Laboratories, which is supported by the Department of Energy under Contract No. DE-AC04-94AL85000.

[1] J. M. Bell and F. K. Cameron, J. Phys. Chem. **10**, 658 (1906).
[2] E.W. Washburn, Phys. Rev. **17**, 273 (1921).
[3] R. Lenormand and C. Zarcone (unpublished).
[4] A. Borhan and K. K. Rungta, J. Coll. Interface Sci. **158**, 403 (1993).
[5] D. A. Nield and A. Bejan, *Convection in Porous Media* (Springer-Verlag, New York, 1992).
[6] F. G. Yost, J. R. Michael, and E. T. Eisenmann, Acta Met. Mater. **43**, 299 (1995).
[7] Copies of the citations for the properties used in Table I are available from J. A. Mann.
[8] L. Romero and F. G. Yost (unpublished).
[9] G. W. Bluman and J. D. Cole, *Similarity Methods for Differential Equations* (Springer-Verlag, New York, 1974).
[10] P. Ehrhard and S. H. Davis, J. Fluid Mech. **229**, 365 (1991).